Physics – Uspekhi **60** (7) 731 – 742 (2017)

PHYSICS OF OUR DAYS

PACS numbers: 68.65.Pq, 71.10.Hf, 73.20.Qt

Quantum melting of a two-dimensional Wigner crystal

V T Dolgopolov

DOI: https://doi.org/10.3367/UFNe.2017.01.038051

Contents

Abstract. The paper reviews theoretical predictions about the behavior of two-dimensional low-density electron systems at nearly absolute zero temperatures, including the formation of an electron (Wigner) crystal, crystal melting at a critical electron density, and transitions between crystal modifications in more complex (for example, two-layer) systems. The paper presents experimental results obtained from real two-dimensional systems in which the nonconducting (solid) state of the electronic system with indications of collective localization is actually realized. Experimental methods for detecting a quantum liquid–solid phase interface are discussed.

Keywords: two-dimensional electron systems, Wigner crystal, semiconducting electron systems

1. Introduction

The term 'Wigner crystal' refers to a crystal which is not made up of ion cores, as usual, but of electrons (or holes). This type of crystal formed of low-density electrons was predicted theoretically [1] as far back as 1934. Clearly, two conditions are necessary for such a crystal to be created. First, a system containing an electron gas should be neutral as a whole. Otherwise, the Coulomb repulsion forces will make the crystal unstable. Second, the characteristic energy of the Coulomb interaction between the electrons, E_C, should greatly exceed the characteristic kinetic electron energy E_k.

The first requirement is most simply satisfied for two-dimensional electron systems (semiconductor devices or an electron layer above a liquid-helium surface [2]), because in this case the compensating positive charge can be located remotely — for example, at a separate electrode. This 'capacitor' arrangement has the additional advantage that it allows the external monitoring of electron density in the two-dimensional layer. The properties of a Wigner crystal in a two-dimensional semiconducting system were first considered in Ref. [3]. It is these electron systems with which we will be concerned below.

As is the case with ordinary crystals, Wigner crystals melt as the temperature increases and the electron system undergoes transition to a liquid phase. For this to occur, the fluctuation of the distance between neighboring electrons due to thermal vibrations should become sufficiently large compared to the crystal's lattice constant. The last statement is in line with the Lindemann criterion [4], which proved quite successful in predicting the melting temperatures of usual crystals. Similar melting can also occur at a temperature close to absolute zero if the zero-oscillation amplitude satisfies the Lindemann criterion — similar to what occurs, for example, in quantum liquids [5]. This kind of melting, referred to as quantum melting, proceeds at a certain critical electron density n_c. In this paper, we consider the features of quantum melting that it exhibits under various conditions in various electron systems.

A special note should be made here to avoid confusion. The existence of a conventional electron liquid at zero temperature is forbidden by the Nernst theorem. In the following discussion, we will assume that the electron system is kept at a sufficiently low temperature for the quantum fluctuations to dominate over the thermal ones but is still able to remain a conventional (or unconventional) Fermi liquid. For a two-dimensional system at a finite temperature, the very notion of a

V T Dolgopolov Institute of Solid State Physics,
Russian Academy of Sciences,
ul. Akademika Osip'yana 2, 142432 Chernogolovka, Moscow region,
Russian Federation
E-mail: dolgop@issp.ac.ru

Received 26 September 2016, revised 20 December 2016
Uspekhi Fizicheskikh Nauk **187** (7) 785 – 797 (2017)
DOI: https://doi.org/10.3367/UFNr.2017.01.038051
Translated by E G Strel'chenko; edited by A Radzig

crystal becomes meaningless for a large-size sample due to the logarithmic divergence of the thermal displacement of an electron from a crystal lattice site. We should therefore confine ourselves to small-size two-dimensional systems (on a 1-cm scale at liquid-helium temperatures).

More complex two-layer systems allow the formation of two-dimensional crystals consisting of electrons from different layers, such that the symmetry of the crystal can be changed by varying the parameters (for example, the electron density). Theoretical predictions concerning phase transitions between various types of crystals at nearly absolute zero are also reviewed in the present paper.

The study of Wigner crystallization is still topical today [6]. The boom in this field at the turn of the 21st century was due both to the improved quality of the structures studied and to newly developed experimental methods (see, for example, Ref. [7]). Notably, all possible simple experiments have naturally been conducted.

The advances of recent years are due primarily to the development of complex and labor-consuming investigation methods [8]. In essence, Jang et al. [8] provided the first reliable demonstration of the existence of acoustic resonances in an electronic 'solid' (and possibly crystalline) phase. The situation where the acoustic resonances manifested themselves most clearly is that of the integer quantum Hall effect close to the filling factor $\nu = 1$ ($\nu = chn_s/(eB)$, where B is the normal component of the magnetic field, n_s is the density of the two-dimensional electron gas, e is the electron charge, c is the speed of light in vacuum, and h is the Planck constant); however, these resonances are also pronounced at noninteger filling factors. The most remarkable point is that in the experiment conducted in Ref. [8] the formation of the crystalline phase does not involve all electrons, but only those excitations that arise in the electron system under conditions where the filling factor differs from the correct integer or noninteger value.

Advances in experimental technology are not the only factor stimulating current research into Wigner crystallization. Novel materials (for example, graphene) have appeared and new ideas emerged on how the solid phase looks in them. A vast field of experimental study arose, lacking thus far both materials of necessary quality and, even more important, experimental methods. Presenting this field requires the analysis of a large body of work, a task which the author attempted to fulfill, if partially, in this paper.

2. Wigner crystal in the absence of a magnetic field

The stability region of the Wigner crystal of an ideal (impurity-free) electron system in a zero magnetic field is estimated applying the Lindemann criterion [9, 10]. For the Coulomb interaction, the characteristic vibrational frequency of electrons about a lattice site is $\omega = [e^2(\pi n_s)^{3/2}/(\varepsilon m^*)]^{1/2}$, where ε is the dielectric constant, and m^* is the electron effective mass. The zero oscillation amplitude is $u = (\hbar\omega m^*)^{-1/2}$. According to the Lindemann criterion, this amplitude is compared at the boundary of quantum melting with the lattice constant: $u = \gamma(\pi n_s)^{-1/2}$, where $\gamma = 0.2-0.25$ is a numerical parameter. As a result, the critical electronconcentration n_c is given by

$$n_c = \left[\pi\left(\frac{a^*}{\gamma^4}\right)^2\right]^{-1}, \qquad (1)$$

with a^* being the effective Bohr radius. Of special note is the fact that, because of the uncertainty in γ, Eqn (1) yields only a crude estimate of the critical concentration. In some calculations (see, for example, Ref. [11]), the value of γ is about two times larger than that given above.

It is expected that a system with electron density above (below) the critical value will be in a liquid (crystalline) state.

If the compensating charge is located at a metal electrode parallel to the two-dimensional electron layer, then at low concentrations the screening by the electrode will establish a new boundary for quantum melting, $n_{c1} < n_c$, below which the interaction will again be weak.

The Coulomb interaction between electrons is commonly characterized by the parameter $r_s = (\pi n_s)^{-1/2}/a^*$. In the simplest case of a single-valley degenerate system in a semiconducting structure, one has $r_s = E_C/E_k$, and the interaction increases as the electron density decreases.

Expression (1) predicts that the electron densities necessary for the formation of a Wigner crystal are extremely low, and hence the values of r_s are extremely large. For example, $n_c \approx 5 \times 10^6$ cm^{-2} for electrons in the GaAs/AlGaAs heterostructure. Theoretical simulations using various methods [12, 13] confirm the small values of n_s, because it is found that the electron–electron separation corresponding to the critical concentration is $37a^*$ ($r_s = 37$). In real two-dimensional electron systems, the transition from a liquid phase to a solid (and hence nonconducting) phase occurs at an electron density two or even three orders of magnitude higher than the theoretical prediction of n_c.

Reference [14] reported calculation of the critical concentration for a Wigner crystal-to-the liquid phase transition in a zero magnetic field in the presence of chaotically distributed impurities with a density of 10^{10} cm^{-2} at a distance of 10 nm from a two-dimensional electron gas. The qualitative result of calculations is that the impurities facilitate the transition to the solid phase. It was found that the critical concentration increased by a factor of 24. The calculation is carried out in such a way that the appearance of a polycrystal is ruled out, and the solid phase is either a single crystal with defects or an amorphous phase. In the neighborhood of the transition point, the solid phase is a single crystal with defects. The authors of Ref. [14], aimed at explaining the results obtained on the high-mobility Si-MOSFET (metal oxide semiconductor field-effect transistor) [15], used the corresponding parameters (electron mass, dielectric constant) and obtained a result close to the experimental value of the critical concentration. There was no awareness at the time of some facts about Si-MOSFET that could greatly affect the critical electron concentration.

Because real impurity-containing systems can, in principle, be totally different from a crystal in the distribution of localized electrons, we will use the term 'solid phase' in discussing such systems

Consider again an ideal electron system. Because the crystallization predicted for such a system must occur for a very strong electron–electron interaction, the question arises automatically whether this strong interaction will allow the electron liquid to remain what it is, just a Fermi liquid we are familiar with. This point was first raised in Ref. [16], which predicted a phase transition that is associated with fermion condensation and can precede Wigner crystallization. According to Ref. [16] and the follow-up publications (see, for example, Ref. [17]), the electron–electron interaction leads to the flattening of the single-particle electronic spectrum in a

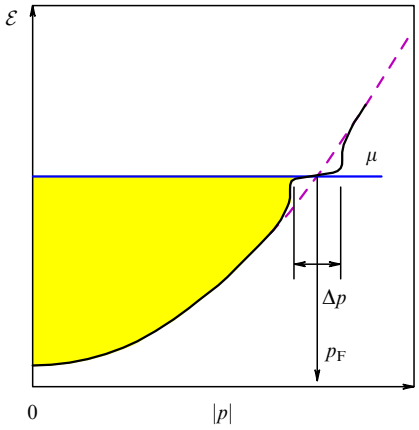

Figure 1. Single-particle electronic spectrum under conditions close to fermion condensation [17].

certain neighborhood of the Fermi momentum p_F, as shown in Fig. 1. An experimental manifestation of this is that the electron effective mass on the Fermi surface increases with decreasing electron density [18]. As a certain concentration n_{FC} is reached, all electrons in the interval Δp turn out to be at the chemical potential level, and the electron liquid ceases to be a Fermi liquid.

Numerical simulations [19] have shown that the effective mass can be made to increase more significantly by introducing impurities; however, the currently available data (see, for example, Ref. [20]) do not support this conclusion.

The increase in the critical concentration on the boundary of the transition from the two-dimensional liquid to the solid phase in a zero magnetic field can be attributed to the influence of impurities in real two-dimensional structures. Two possible scenarios are the following: a direct transition from the Fermi liquid to the solid nonconducting phase ($n_c > n_{FC}$), and a two-step Fermi liquid–fermion condensate–solid phase transition ($n_c < n_{FC}$). There is no knowledge yet of the properties of the electron system after the first phase transition in the presence of impurities. The only reliable observation is that, in all the experiments done, the solid phase is a collective phenomenon and has no relation to the single-particle electron localization.

3. General picture in a normal magnetic field

Research into Wigner crystals in two-dimensional electron systems placed in a normal magnetic field was begun historically by Fukuyama [9] and Lozovik and Yudson [10]. According to Ref. [10], in an impurity-free electron system the quantum melting of the Wigner crystal in strong magnetic fields should occur at an electron concentration proportional to the magnetic field value, with proportionality factor $2\gamma^2$, where γ is a parameter involved in the Lindemann criterion. Thus, the quantum melting boundary in a strong magnetic field corresponds to the filling factor $\nu \approx 0.1$ (Fig. 2). A similar result ($\nu \approx 0.15$) was obtained in Ref. [21].

The linear dependence of the quantum melting boundary was observed repeatedly in various two-dimensional electron systems [22–26], but in none of the known experiments was the filling factor corresponding to the boundary slope so small.

It would seem that the slope of the liquid–solid phase interface is not exact due to model built in Ref. [10], which

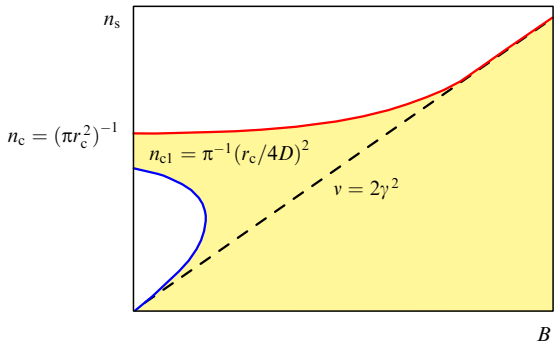

Figure 2. (Color online.) Quantum melting boundary according to Ref. [10]. Here, $r_c = a^*/\gamma^4$, and D is the distance to the gate. The dark region corresponds to the Wigner crystal.

assumed that all electrons at a lattice site vibrate independently and at the same frequency, similar to Einstein's thermal conductivity model. In reality, the vibrations of the electronic lattice are collective and dispersive. Taking this into account [27] decreases the interface slope by another factor of two.

As already mentioned, in a zero magnetic field in two-dimensional systems with a metal electrode, a decrease in the electron density to below n_c can lead to originating a new melting process (blue line in Fig. 2) due to the Coulomb interaction screening by the gate. Indeed, because the distance to the metal electrode is determined during the sample preparation process, it follows that, under the condition $2D < r_c$, a Wigner crystal will not exist at all in a zero magnetic field; in the ideal case, it will only appear in a sufficiently strong magnetic field. The phase diagram in Fig. 2 corresponds to the inequality $2D > r_c$. The region of existence of the liquid phase embraces a certain region in the (B, n_s) plane, and the interface for $B \to 0$ has the same asymptote as in strong fields.

4. Mixing of quantum levels in a weak quantizing magnetic field

The position of the quantum melting boundary is significantly affected by the ratio between the cyclotron and Coulomb energies. If the Coulomb electron–electron interaction energy exceeds the cyclotron energy, we can no longer treat each electron as being in the lowest quantum state, nor can we apply the Lindemann criterion to zero-point oscillations as in Ref. [10].

The determining parameter for the mixing of states at various quantum levels is defined as follows:

$$\alpha = \frac{e^2(\pi n_s)^{1/2}}{\varepsilon\hbar\omega_c} = \frac{\nu r_s}{2}\,. \qquad (2)$$

Shown by the red dashed line in Fig. 3 is the curve ($\alpha = 1$) that divides the (B, n_s) plane into two regions, in one of which the mixing of quantum levels is important. To the left of the point where this curve intersects the straight line $\nu = 2\gamma^2$, quantum level mixing changes appreciably the position of the quantum liquid–solid phase boundary. Of particular interest are noninteger filling factors with an odd denominator. It is shown in Ref. [31] that, as a result of quantum level mixing, a liquid phase in the fractional quantum Hall effect (FQHE) regime may be less favored energetically than a liquid phase,

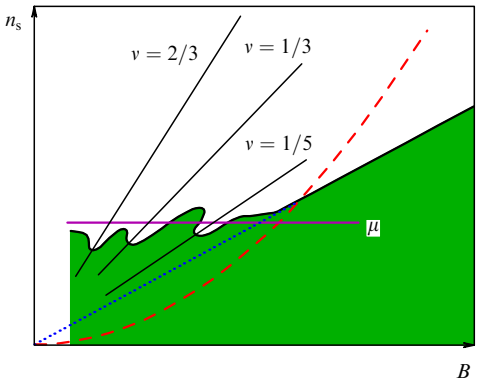

Figure 3. (Color online.) Schematic of the interface between the quantum liquid and Wigner crystal (dark region) in a magnetic field, taking into account quantum level mixing. Even in an ideal electron system, quantum level mixing due to the Coulomb interaction [28–30] changes significantly the position of the quantum melting boundary.

which can cause the interface to oscillate, as shown qualitatively in Fig. 3. A similar phase diagram obtained from empirical considerations was recently displayed in Ref. [32].

Despite the very long history of experimental investigations, no reports are available on the direct observation of the oscillation of the quantum liquid–Wigner crystal interface in the FQHE regime (the only — though not very convincing — exception being Ref. [33]). On the other hand, the literature abounds with reports on the re-entrant dielectric phase in the FQHE regime [34–39]. How the re-entrant behavior occurs in the range of the filling factor $\nu = 1/5$ is illustrated in Fig. 3, where the quantity μ corresponds to the chemical potential level in a zero magnetic field. In the FQHE regime, the chemical potential exhibits slight oscillations [40], which we ignore here for simplicity.

As illustrated in Fig. 3, in the region of a relatively weak magnetic field, a two-dimensional electron system resides in the state of a quantum liquid. In a magnetic field exceeding that corresponding to the filling factor $\nu = 1/3$, the ground state is the crystalline state which ceases to exist and becomes a quantum liquid in the neighborhood of the filling factor $\nu = 1/5$. Clearly, depending on the position of the chemical potential, similar behavior can also be realized for other fractional filling factors.

Both interface oscillations [24, 25, 41] (Fig. 4) and re-entrant behavior [42] were observed experimentally in two-

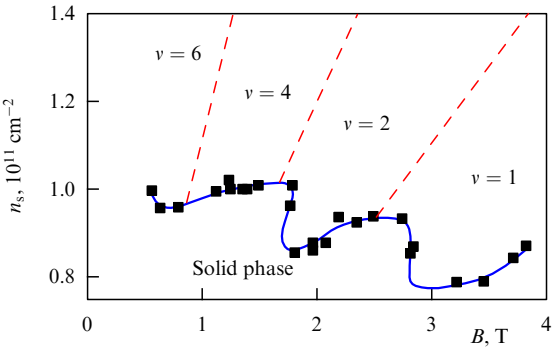

Figure 4. Experimental observation of the quantum liquid–solid phase interface oscillations in the region of the integer quantum Hall effect in Si-MOSFET (100). (Data taken from Ref. [41].)

dimensional electronic systems of silicon field effect transistors for integer filling factors.

An attempt at a theoretical explanation of interface oscillations in the region of the integer quantum Hall effect was undertaken in Ref. [43] under the assumption that at the quantum liquid–solid phase interface both phases coexist, and hence the electron chemical potentials in these two phases are equal, namely

$$\mu_S(n_c) = \mu_L(n_c, B)\,. \tag{3}$$

The chemical potential of the solid phase in a magnetic field remains constant (or varies weakly monotonically), whereas the chemical potential of the liquid oscillates. Expanding Eqn (3) up to first-order corrections and taking into account that the chemical potentials in a zero magnetic field are equal, we obtain

$$\delta n_c = \delta\mu(B)\left[\left(\frac{\mathrm{d}\mu_S}{\mathrm{d}n_s} - \frac{d\mu_L}{\mathrm{d}n_s}\right)_{n_c,\,B=0}\right]^{-1}. \tag{4}$$

As seen from Eqn (4), the phase and amplitude of interface oscillations are determined by the compressibility difference between the liquid and solid phases.

The compressibility of the liquid phase at such a low density as n_c is negative. The compressibility of the solid phase is determined by the same Coulomb interaction and is also negative, but the compressibility of the liquid phase is larger in absolute value; therefore, the phase of the interface oscillations coincides with that of the oscillations of the liquid chemical potential. As shown in Ref. [43], expression (4) gives a correct order of magnitude value for interface oscillations, while failing to fully describe their shape.

5. Strong normal magnetic field

We now consider the opposite limit, $\alpha < 1$. As shown in Figs 2 and 3, it is expected that the boundary will tend to an asymptote which passes through the origin of coordinates and whose slope corresponds to the filling factor $\nu \approx 0.1$.

Measured boundary positions in high-mobility (2×10^6 to 8×10^6 cm^2 V^{-1} s^{-1}) heterostructures GaAs/AlGaAs are demonstrated in Fig. 5. The first point to note is that the re-entrant behavior of the boundary is observed in the magnetic field region where quantum level mixing is of no importance. The dashed line in Fig. 5 marks the boundary of the strong quantum level mixing. To the left of it, mixing is weaker. Still, this region exhibits a re–entrant behavior of the solid phase, as illustrated in Fig. 5 with data from the same Ref. [22] (in the main figure, the corresponding points are shown by triangles).

The observation of re-entrant behavior in this region can be attributed either to the large numerical factor on the right-hand side of expression (2) or to the fact that quantum level mixing is not the primary mechanism for the oscillations of the solid–liquid phase interface, or else to the fact that re-entrant behavior has no relation to interface oscillations.

The strong-field boundary indicated in Ref. [22] (solid line in Fig. 5) is indeed close to a straight line, but its slope is about two times larger than expected. Moreover, contrary to theoretical predictions, the straight line does not pass through the origin of coordinates. If we allow for the possibility of an oscillating phase interface, the solid line is not a true phase interface in strong magnetic fields. The true

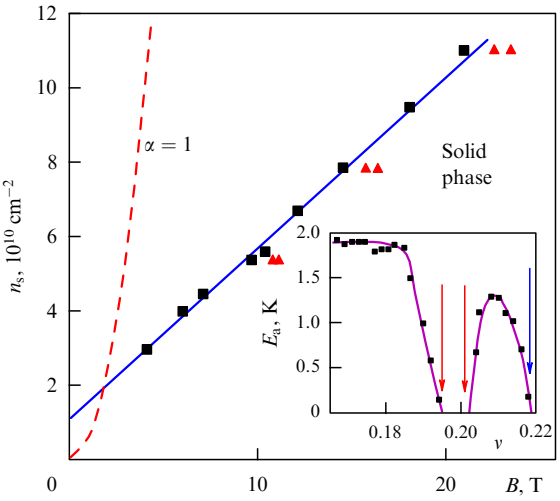

Figure 5. Solid–liquid phase boundary obtained from the data taken from Ref. [22]. The dashed line marks the boundary of strong quantum level mixing. The inset shows the dependence of the activation energy on the filling factor for the highest electron density specimen; the arrows label the points corresponding to the phase boundaries.

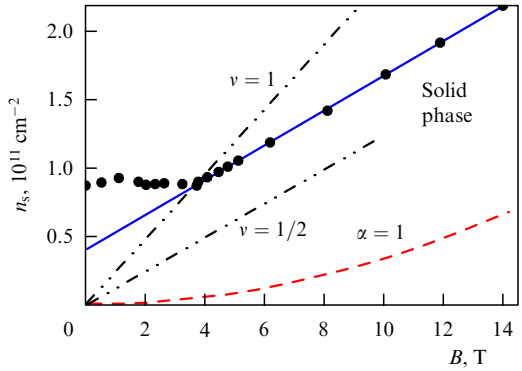

Figure 6. Liquid–solid phase boundary in Si-MOSFET (100) (data taken from Ref. [24]). The marked lines correspond to the filling factors of 1 and 1/2, and also to $\alpha = 1$.

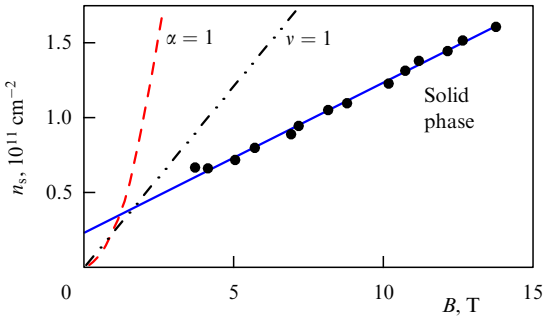

Figure 7. Boundary (solid line) between the liquid and solid phases in an InGaAs quantum well. Also shown are the line ($\alpha = 1$) separating the region of strong quantum level mixing from the region of weak mixing and the straight line corresponding to a filling factor of unity ($\nu = 1$).

boundary should be determined by a line drawn through the triangle points lying to the right.

A solid–liquid phase boundary in a high-mobility silicon MOSFET structure was measured in Refs [23, 24]. The data of Ref. [24] are presented in Fig. 6. The specimen studied, with the mobility range of 20,000–30,000 cm^2 V^{-1} s^{-1}, did not exhibit the fractional quantum Hall effect, so there is no reason to expect boundary oscillations similar to those shown in Fig. 3. As mentioned (see Fig. 4), oscillations at integer filling factors occur. As the magnetic field is increased and the boundary crosses the value $\nu = 1$, the boundary becomes a straight line. Similar to the GaAs/AlGaAs heterostructure, the straight line does not pass the coordinate origin. The slope of the straight line is close to the filling factor $\nu = 1/2$ (see Fig. 6).

While apparently similar, the results from Si-MOSFET and GaAs/AlGaAs heterostructures are considerably different: in the former case (see Fig. 6) and in the latter case (see Fig. 5), quantum level mixing is, respectively, strong and weak in the region where the straight-line boundary passes.

To check that the shape of the solid–liquid phase boundary depends only weakly on quantum level mixing, we conducted measurements on $In_{0.75}Ga_{0.25}As$ quantum wells 20 nm in thickness sandwiched between $In_{0.75}Al_{0.25}As$ barriers.[1] The two-dimensional electron gas in these structures exhibited strong Rashba spin–orbit coupling [44, 45] and a mobility of 3×10^5 cm^2 V^{-1} s^{-1}. From a comparison of Figs 6 and 7, the main difference between the electrons in the InGaAs quantum well and in Si-MOSFET is in the degree of quantum level mixing in the region of measurement. Despite this difference, the experimental results are similar: the boundary is a straight line, it does not pass through the origin of coordinates, and its slope greatly exceeds the expected theoretical value.

In concluding this section, it is worthwhile to note that all known experimental results for a strong magnetic field disagree with theoretical expectations. First, the slope of $n_c(B)$ turned out not to be universal. Second, the straight line $n_c(B)$ in the (n_s, B) plane does not pass through the coordinate origin. There is a simple physical justification for the requirement that n_c be proportional to B: in strong fields, the amplitude of zero-point oscillations is inversely proportional to the magnetic field. Linearity (rather than proportionality) might only occur if some of the electrons localize on positively charged centers with a localization radius significantly shorter than the lattice constant of the Wigner crystallites.

6. Wigner crystal in graphene

In this section and also in Sections 7–11, we will consider 'solid' electronic phases in materials that have only relatively recently become subjects of research — the reason why theoretical studies on them abound, whereas experimental studies are virtually absent. Information on these theoretical results will be of use to experimentalists in formulating a problem and developing necessary investigation methods.

We begin with a single-layer crystal of graphene, i.e., a graphite monolayer, lying on a dielectric substrate or freely suspended. The spectrum of charge carriers is such that the electron and hole bands touch each other in the corners of the hexagonal Brillouin zone. There are two independent spectral branches within the Brillouin zone, each with a spectrum in

[1] Thanks are due to M Yu Mel'nikov, A A Shashkin, G Biasiol, and L Sorba for kindly allowing the author to use the structures they grew in preparing his measurement specimens.

the form

$$\mathcal{E}(k) = \hbar v_G k\,, \tag{5}$$

where the wave vector k is measured from the point of touch, and the velocity v_G is on the order of 10^8 cm s^{-1}. Such a spectrum is called 'massless'. The two-dimensional system of charge carriers in graphene is ideal in the sense that the wave function in the direction normal to the plane has the least possible size.

In Ref. [46], it is shown that no Wigner crystal can exist in a single-layer graphene in a zero magnetic field. To see that this is indeed so, note that a prerequisite for the existence of a Wigner crystal is that the potential energy of repulsion between charged particles, E_C, greatly exceed the kinetic energy of zero-point oscillations: E_k, $E_C \gg E_k$. For a quadratic spectrum, this condition is equivalent to condition (1).

In a graphene Wigner crystal with an interparticle separation L, the potential energy in a region of area A is $E_C = n_s A e^2/(\varepsilon L)$, and the corresponding kinetic energy is $E_k = \hbar v_G (2\pi/L) n_s A$. Because the energy ratio

$$\frac{E_C}{E_k} \simeq \frac{e^2}{h\varepsilon v_G} \tag{6}$$

is independent of the electron density, the existence of Fermi liquid in graphene implies the absence of a Wigner crystal. Furthermore, because the dielectric constant can only be increased, it is impossible to achieve crystallization by varying ε. It remains possible to decrease v_G, which can be done by applying a mechanical stress to the graphene layer. However, achieving Wigner crystallization requires a more than an order of magnitude decrease in velocity, which does not seem possible.

The absence of Wigner crystallization in a zero magnetic field does not at all imply its absence in strong fields. In a quantizing magnetic field, two ladders of quantum levels exist in single-layer graphene with different pseudospin indices corresponding to different valleys. Valley splitting is comparable to cyclotron splitting; therefore, the quantum levels can be presented by the following relations (see, for example, Ref. [47]):

$$\begin{aligned} E_n^{u} &= \operatorname{sign} n \, \frac{h v_G}{2\pi l} \left(2|n|\right)^{1/2}, \\ E_n^{d} &= \operatorname{sign} n \, \frac{h v_G}{2\pi l} \left(2|n+1|\right)^{1/2}, \end{aligned} \tag{7}$$

where $l = [\hbar/(eB)]^{1/2}$ is the magnetic length. Notice that each of the levels in formulas (7) is also doubly spin-degenerate.

The question of the possibility of current carrier crystallization in a system with spectrum (5) was considered in Ref. [48]. While this work has certain limitations (it ignores the possibility of the fractional quantum Hall effect, disregards quantum level mixing, and limits the mean field method to the filling factors of those regions which exhibit a strong correlation between current carriers with different pseudospin indices from different valleys) and its conclusions have not been verified in experiments, it is of interest, however, because it not only predicts the possibility of the existence of a Wigner crystal but also demonstrates a variety of crystalline phases with phase interfaces between them.

The authors of Ref. [48] differentiate between a usual Wigner crystal with one Fermi particle per unit cell, a so-called bubble phase with two ($N = 2$) and three ($N = 3$) particles per unit cell, and strip phases reminiscent of charge density waves.

Calculations made in Ref. [48] show, for example, that in the filling factor range corresponding to the lower, $n = 2$, quantum level the following sequence of crystalline phases is expected to occur as the filling factor is increased: a Wigner crystal, an $N = 2$ bubble crystal, and a strip crystal. At the next Landau level, the $N = 3$ bubble crystal interferes the phase competition.

Each of these phases should disappear with decreasing magnetic field even if the filling factor is fixed. The question of the boundaries of the existence of crystalline phases in a magnetic field was not considered in Ref. [48]. Later on, the same authors showed in paper [49] that the mixing of Landau levels in graphene causes no significant change in the phase diagram.

In Ref. [50], the idea was advanced that, in addition to the nonuniform charge distribution, a set of pseudospin structures and meron crystals may develop in graphene. The energies of different meron crystals were compared among themselves and with the Wigner crystal and bubble crystal energies to support this idea.

The simplest way to experimentally check the predictions of Refs [48, 49] is to use Corbino-shaped graphene samples. In the neighborhood of the corresponding filling factor, even a slight change in the activation energy due to a phase transition should show up as the maximum of the measured inverse conductivity $1/\sigma_{xx}$.

7. Two-layer graphene

In recent years, two-layer graphene (Fig. 8a) has come under research scrutiny by theoretical physicists concerned with Wigner crystallization in graphene. This material is composed

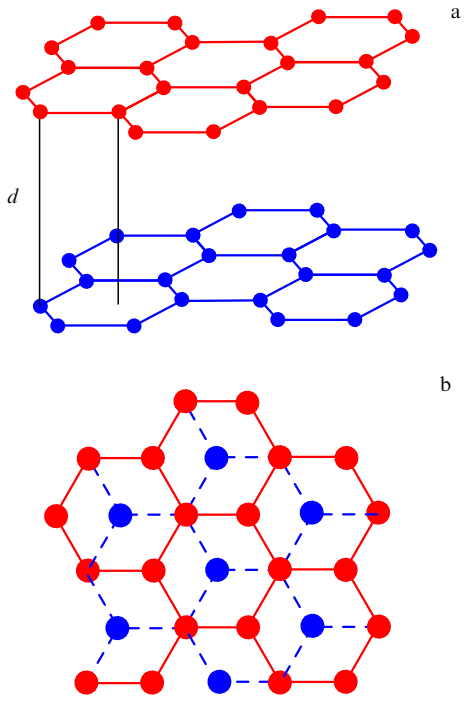

Figure 8. (a) Crystal structure of two-layer graphene in the Bernal AB packing configuration The interlayer distance is $d = 0.335$ nm. (b) Projection of two-layer graphene onto the base plane.

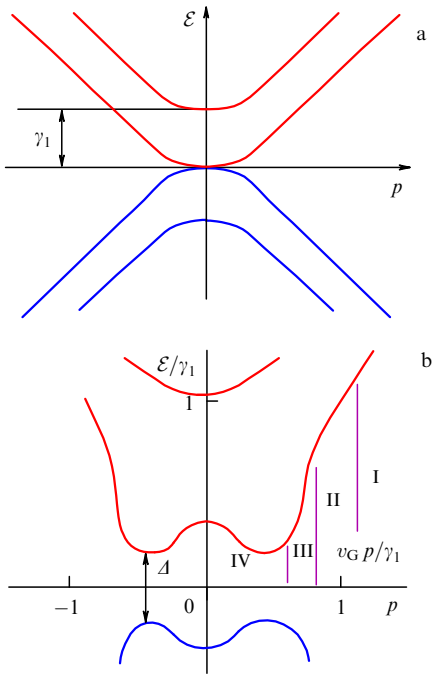

Figure 9. Schematic spectrum of two-layer graphene: (a) in the absence of an electric field, and (b) in the presence of a potential difference applied across the layers.

of two closely spaced graphene layers. In the absence of interlayer tunneling, its spectrum would be exactly the same as that of single-layer graphene with an additional double degeneracy.

From Fig. 8b it is seen that the base plane projections of some of the sites in the two layers coincide, and tunneling over these sites removes the additional degeneracy. The result of the tunneling is, in addition to the removed degeneracy, the disappearance of the conic point. The spectrum (Fig. 9a) remains gapless with finite but small carrier mass ($m = 0.033\,m_0$, where m_0 is the free-electron mass).

Can a system with such a spectrum make a transition to a crystalline state, and if it can, what will be the electron density distribution? An attempt to answer these questions was made in Ref. [51] by numerically analyzing the equilibrium distribution of electron density over various lattice sites of two-layer graphene in a strong-coupling model. The variable parameters were the average electron density at a site, the probability of interlayer tunneling, and the Coulomb potential. It is shown that there is a region of parameters where a nonuniform electron distribution over the sites can be treated as Wigner crystallization. The existence of two phases is shown to be possible. To the author's knowledge, there has been no follow-up to Ref. [51], either theoretical or experimental.

One way to produce a gap in the spectrum of two-layer graphene is to apply an electric potential V across the layers, with the necessary result that the current carrier concentration will be different in the layers. The magnitude of the gap is governed by the applied voltage:

$$\Delta = eV\left(\frac{\gamma_1^2}{\gamma_1^2 + e^2V^2}\right)^{1/2}. \tag{8}$$

Figure 9b shows a schematic of the spectrum of two-layer graphene in the presence of a voltage across the layers.

Two-layer graphene with a voltage applied across the layers is more convenient for experiment. Various versions of Wigner crystallization in this material are considered theoretically in Ref. [52]. We will restrict ourselves to the lowest electron subband. We divide the energy axis into four intervals as follows (Fig. 9b):

$$\begin{aligned}
&\text{(I)}\ \ \mathcal{E} \approx v_G\,p\,, \quad v_G\,p \gg \gamma_1\,;\\
&\text{(II)}\ \ \mathcal{E} \approx \frac{v_G^2\,p^2}{\gamma_1}\,, \quad (eV\gamma_1)^{1/2} \ll v_G\,p \ll \gamma_1\,;\\
&\text{(III)}\ \ \mathcal{E} \approx eV + \frac{v_G^4\,p^4}{2eV\gamma_1^2}\,, \quad eV \ll v_G\,p \ll (eV\gamma_1)^{1/2}\,;\\
&\text{(IV)}\ \ \mathcal{E} \approx eV - \frac{2v_G^2\,p^2}{\gamma_1^2} + \frac{v_G^4\,p^4}{2eV\gamma_1^2}\,, \quad v_G\,p \approx eV\,.
\end{aligned} \tag{9}$$

Within interval I, i.e., for high energies and large electron concentrations, the layer-to-layer coupling is weak, the spectrum is linear, and the Coulomb interaction has the same form as in a single-layer graphene. No Wigner crystal can exist in this interval.

In interval II, charge screening is an important factor. The Coulomb energy has the form $E_C(r \gg 1/q_{TF}) \simeq e^2/[(q_{TF}r)^2 r]$, where $(q_{TF})^{-1} \approx \hbar v_G/(2p\gamma_1)$ is the Thomas–Fermi screening length. It is clear that the Coulomb energy cannot exceed the kinetic energy in this interval, so that here also Wigner crystallization is impossible.

In interval III, the spectrum of the electron system of a two-layer graphene has a gap and hence is similar to that of an insulator. The screened Coulomb interaction takes the form

$$E_C\left(r \gg \frac{\hbar v_G}{(eV\gamma_1)^{1/2}}\right) = \frac{3eV}{4}\ln\frac{\hbar v_G}{eVr}\,. \tag{10}$$

The electron–electron interaction closely resembles the interaction between Abrikosov's vertices in a superconductor which, as is known, form a triangular lattice.

The quantum melting boundary in interval III is determined in Ref. [52] using a Hamiltonian with effective interparticle interaction defined by Eqn (10). According to the Lindemann criterion, the boundary is specified by the condition

$$a \gg \frac{dg_0}{(eV\gamma_1)^{1/2}}\,, \tag{11}$$

where a is the crystal lattice constant, and $g_0 = 2\hbar v_G/(3d) = 2.8\,eV \gg \gamma_1 = 0.39\,eV$. Because a determines the electron density, condition (11) gives the upper boundary of quantum melting.

Further lowering the electron density causes a transition to interval IV, where another change in screening occurs and a symmetry-changing structural transition crystal–crystal takes place. The last transition is determined by the condition $a \approx dg_0\gamma_1/(eV)^2$. Figure 10 shows the electron density distribution in the neighborhood of lattice sites.

A distinctive feature of two-layer graphene in interval IV is a sombrero-shaped single-particle electronic spectrum. A convenient way to consider how and why such a spectrum leads to a nontrivial electron density distribution in Wigner crystal sites is through the example of a one-layer electron system with a strong spin–orbit coupling.

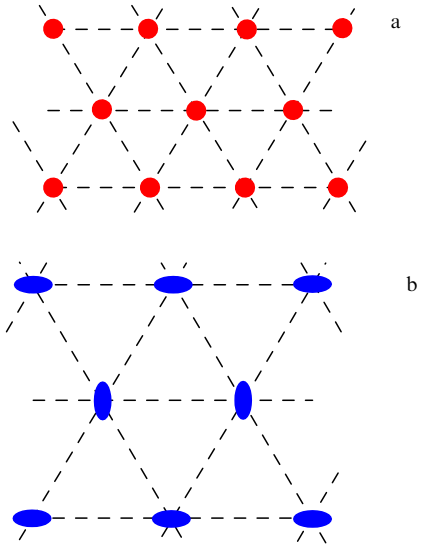

Figure 10. Schematic of electron density in a Wigner crystal for intervals III (a) and IV (b). (Results taken from Ref. [52].)

8. Wigner crystal in a system with strong spin–orbit coupling

In this section, we will consider an electron gas with a strong Rashba type spin–orbit coupling. The kinetic part of the Hamiltonian assumes the form

$$\sum_i H_{0i} = \sum_i \left(\frac{p_i^2}{2m} + \lambda(\sigma_x p_{yi} - \sigma_y p_{xi}) - \frac{m\lambda^2}{2} \right), \qquad (12)$$

where λ is the spin–orbit coupling constant, and $\sigma_{x,y}$ are the Pauli matrices. The solution of the Schrödinger equation with this Hamiltonian is the single-particle spectrum shown in Fig. 11a. The electron spin is normal to the electron momentum, and the points of minimal energy in p-space form a circle of radius $m\lambda$.

The potential part of the Hamiltonian is expressed as

$$\sum_{i<j} \frac{e^2}{|\mathbf{R}_{ij} + \mathbf{r}_{ij}|}. \qquad (13)$$

Here, $\mathbf{R}_i$ specifies the position of a site in the triangular a-periodic lattice, $\mathbf{r}_i$ is the displacement of the electron from the corresponding site. If the Coulomb interaction is strong and a crystal forms, the oscillation frequency around a lattice site is of order

$$\omega_0 \simeq \left(\frac{e^2}{ma^3} \right)^{1/2}, \qquad (14)$$

in accordance with Eqn (13).

In what follows, it is assumed that the spin–orbit coupling is strong and

$$m\lambda^2 \gg \hbar\omega_0\,; \qquad (15)$$

hence, the Wigner crystal borders a liquid, which occupies in p-space a narrow strip near the circle $|p| = m\lambda$. The usual condition $e^2/a \gg \hbar\omega_0$ is assumed to be satisfied.

Here, a question unintentionally arises: are not the above inequalities contradictory? It is a matter of simple arithmetic

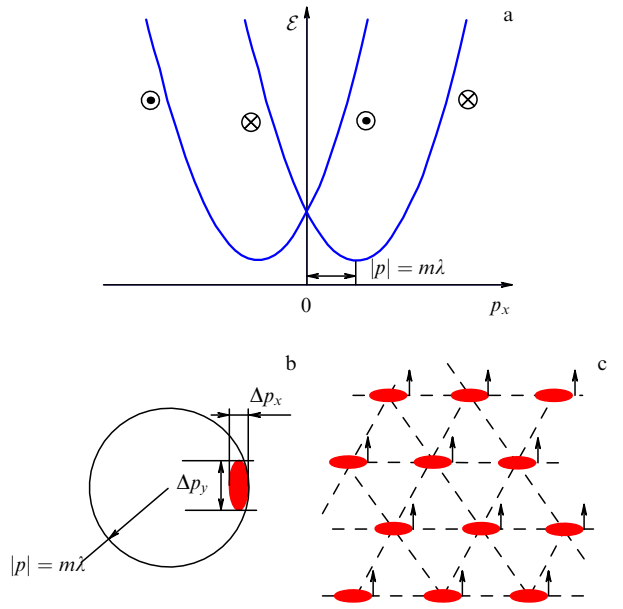

Figure 11. (a) Spectrum of an electron system with a strong Rashba type spin–orbit coupling. (b) Formation region of a wave packet in momentum space. (c) Symbolic depiction of a Wigner crystal with asymmetric electron density distribution at lattice sites, with arrows showing the electron spin orientation.

to show that they are consistent if the condition

$$\lambda \geqslant \frac{e^2}{\varepsilon\hbar} \qquad (16)$$

holds. A realization of a two-dimensional Rashba type-coupled electron system meeting condition (16) has been reported recently [45].

The following discussion refers equally to systems like the ones we consider in this section and to all two-dimensional electron systems with the 'sombrero'-shaped spectrum. We will build a crystal by placing a packet of single-particle electronic wave functions at each site. To do this, all states within the strip near a circle $|p| = m\lambda$ could be used. The zero-point oscillation energy of such a symmetric wave packet would be determined by the quantity Δp:

$$(p - m\lambda)^2 < \Delta p^2 \simeq \left(\frac{e^2\hbar^2 m}{a^3} \right)^{1/2} \ll (m\lambda)^2. \qquad (17)$$

However, the zero-oscillation energy can be reduced if we break the wave packet symmetry, for example, as shown in Fig. 11b. Taking $\Delta p_x \ll \Delta p$ will extend the electron wave function in the x-direction in real space. For the y-direction, accordingly, the formation of a wave packet will require the momentum interval defined by $m\lambda \gg \Delta p \gg \Delta p_x$, which will not increase the zero-oscillation energy noticeably, because the magnitude of $\langle H_{0i} \rangle$ is minimal along the circle $|p| = m\lambda$ (see Fig. 11). As for the change in the potential energy due to the x-extension of the wave function, its small value compared to the zero-oscillation energy imposes the limitation on $\Delta x \simeq [a^3\hbar^2/(me^2)]^{1/4}$.

Clearly, the system of parallel-extended ellipsoidal wave packets at crystal lattice sites shown in Fig. 11c is not the only possibility [53]. Possible alternatives are, for example, crystals of ellipsoids oriented orthogonally, as shown in Fig. 10b or of ellipsoids rotated by 120°, the latter case suggesting possible transitions between various crystalline phases in systems with

a strong spin–orbit coupling. Electron systems with screened interaction provide even more possibilities for constructing various crystalline phases [54].

The major problem in studying strongly spin–orbit–coupled systems experimentally is reaching very low electron densities and, hence, ensuring high quality. Only the most perfect systems could exhibit the slight effects described above. The most convenient candidates would be InAs and InGaAs quantum wells with InAlAs barriers. Unfortunately, existing materials of this type are insufficiently perfect; even the best of them exhibit a percolation transition from the conducting to nonconducting phase due to residual disorder.

9. Two-layer electron systems

Let us consider an electron system consisting of two parallel layers with the same electron density separated by a distance d. It will be assumed that (1) the total electron concentration n_s is less than half the critical concentration, $n_s < n_c/2$, (2) the system is ideal, (3) the Coulomb interaction is unscreened [55–63], and (4) the interlayer tunneling is negligible.

An electron system like this can be realized in a double quantum well with a narrow nonconducting barrier. The equality of concentrations is achieved by using two gates located on opposite sides of the well at a distance significantly exceeding the electron–electron separation.

The ground state of the system is determined by the Coulomb energy minimum which depends on the parameter $\eta = dn_s^{1/2}$. It is clear that the crystal lattice will be triangular, both at very small and very large interlayer separations, but in the former case the lattice consists of electrons from different layers (Fig. 12a), while in the latter case, only of electrons from each layer (Fig. 13b). According to numerical calculations, increasing the interlayer distance causes a second-order transition at $\eta = \eta_1$, after which the lattice in both layers becomes rectangular with $1 < a_1/a_2 < \sqrt{3}$ (Fig. 12b). The next second-order transition will occur at $\eta = \eta_2$ (Fig. 12c)

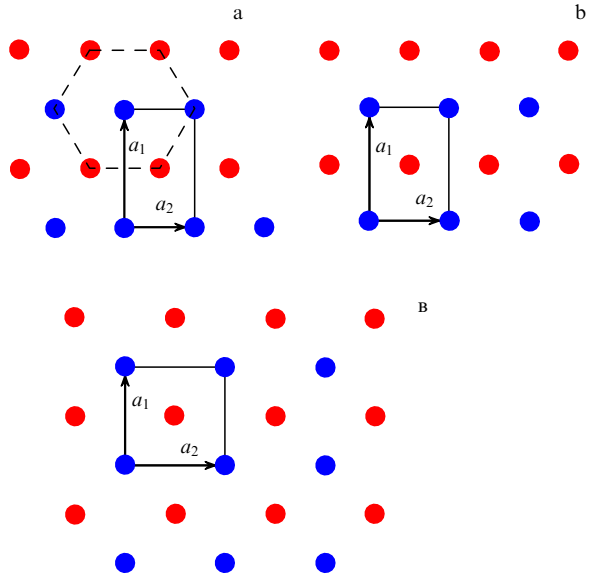

Figure 12. Initial evolution of the Wigner crystal in a two-layer system with increasing interlayer distance. (a) Triangular lattice composed of electrons from different layers. Shown is a unit cell for electrons from one layer, $a_1/a_2 = \sqrt{3}$. (b) Rectangular unit cell in each layer, $1 < a_1/a_2 < \sqrt{3}$. (c) Square unit cell in each layer.

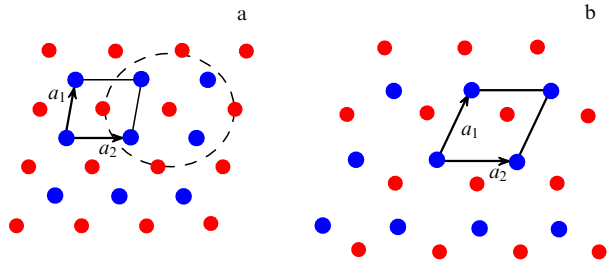

Figure 13. Follow-up evolution of the Wigner crystal in a two-layer system with increasing interlayer distance.

and the lattice in each layer will become square and will remain so for η until the value $\eta = \eta_3$, when another second-order transition occurs, and at $a_1 = a_2$ the angle between the basis vectors will start changing (Fig. 13a). At $\eta = \eta_4$, the lattice in each of the layers becomes a triangle (Fig. 13b).

However, if $n_c/2 < n_s < n_c$, the chain of quantum transitions between solid phases can be interrupted by melting. Interestingly, in the described chain of Wigner crystals the modification shown in Fig. 12c turns out to be the most stable toward thermal melting [64].

In a quantizing magnetic field at filling factors below unity, the spatial structure of the Wigner crystal is described by the same five-stage scenario illustrated in Figs 12 and 13 [65]. Including even weak interlayer tunneling will lead to more complex, diverse, and filling-factor-dependent phase diagrams, with variations not only in the spatial position of lattice sites but also in the composition of each site from electrons appertaining to different layers (pseudospin state of a site). A detailed discussion of these diagrams makes no sense because of the current lack not only of experiments in this field but also of ideas on how theoretical predictions can be checked.

10. Methods for detecting a liquid–solid phase interface

The most convincing method for detecting quantum melting experimentally would be by observing transverse waves traveling through the crystal and registering the conditions in which they disappear due to melting. An observation of transverse oscillations in a solid phase was reported in an early publication [66] but was soon disproved [67]. No successful application of the method has been reported to date, most probably because of the imperfect solid phases the researchers work with. Even when investigating most perfect two-dimensional electron systems, there is no confidence that the object under study has a single-crystal nature. Many experiments performed have used other methods that do not require any long-range order in the solid phase.

It is found that the dissipative conductivity in a solid phase is of the activated type. Measuring the evolution of the electron density dependence of the activation energy, $E_a(n_s)$, as the system approaches the solid–liquid phase boundary provides the boundary concentration via extrapolating the activation energy to zero. While conceptually simple, however, this method requires great effort, because to determine the activation energy for each electron density it is necessary to measure the temperature dependence of the conductivity and to obtain a sufficient number of points in the $E_a(n_s)$ dependence to be able to extrapolate reliably. And all this, only to obtain one point at the boundary.

A less labor-consuming, although more poorly grounded method for obtaining the boundary from transport data, is to study the nonlinear properties of the solid phase at a temperature on the order of 10 mK. At these temperatures, the volt-ampere characteristics of the solid phase demonstrate a threshold behavior in the voltage interval which smoothly decreases on approaching the phase interface. The extrapolation to zero of the concentration dependence of the threshold voltage yields the boundary values of the electron density. Both transport methods give the same boundary concentrations to within their accuracies [68].

A further and the most rapid 'semiquantitative' method for constructing the solid–liquid phase boundary should be noted here. With this method, the only thing to do is to mark, at a sufficiently low temperature (≈ 30 mK), the concentration at which the dissipative conductivity is already small (for example, $0.1e^2/h$). The conductivity decreases so rapidly away from the boundary that the coefficient of e^2/h does not shift the boundary value of the concentration anywhere significantly.

To detect the emergence of a solid phase in a single heterojunction GaAs/AlGaAs, the authors of the experiments in Refs [7, 69] (who assumed this phase to be a Wigner crystal) also used an optical method, which consists in observing the spectrum of radiative recombination of 2D electrons with holes placed in the acceptor delta-layer. It is shown that at low temperatures in strong magnetic fields these spectra exhibit an additional line shifted towards lower energies (Fig. 14). There are many indications — including behavior with temperature and suppression at fractional filling factors, etc. — that this line can be ascribed to the luminescence of electrons in the solid phase, even though the liquid–solid phase boundary given in Ref. [7] differs from that obtained from the data reported in Ref. [22]. This difference can be a fundamental one, because optical experiments measure bulk properties, whereas transport experiments examine the properties of the percolation grid (if the system of current carriers is nonuniform).

And finally, there is yet another possibility of detecting the liquid–solid phase boundary. In Refs [70–75], it is shown that when exciting a solid phase by a radio-frequency signal in strong magnetic fields resonances can be observed that can be interpreted as the resonance vibrations of a pinned Wigner crystal. The boundary can be constructed from the resonance disappearance points.

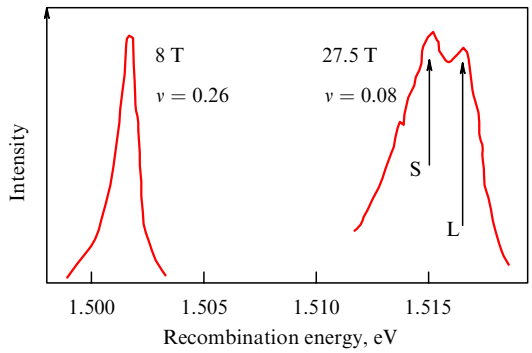

Figure 14. Normalized luminescence spectra at an electron concentration of 5.4×10^{10} cm^{-2} in various magnetic fields. Line L corresponds to the liquid phase, and line S presumably refers to the solid phase. (Data taken from Ref. [7].)

The response of a two-dimensional electron system to radio-frequency excitation can also be examined in experiments on the propagation of surface acoustic waves. These experiments allow working with highest-mobility systems without screening the Coulomb interaction between electrons and also permit moving away from the boundary into the depth of the solid phase [76]. Unfortunately, despite its obvious promise, this method has failed to demonstrate any advantages over other investigation methods.

11. Intermediate phases

The Lindemann condition, while specifying the stability boundary of the crystalline state, by no means determines what will happen to the system of current carriers after melting. Many theoretical proposals exist on possible intermediate phases between a classical Fermi liquid and a crystal. One such intermediate phase, a fermion condensate, was discussed in Section 1. The possible appearance of a highly correlated intermediate phase was first mentioned in Ref. [77], which discusses the existence of a liquid of freely traveling defects in a crystal. For the case of the conventional thermal melting of a Wigner crystal, it is assumed in Ref. [78] that it first loses translational order but retains orientational order (transition through a 'hexatic' state). A similar scenario is also possible for quantum melting. It remains unclear whether and how the transport properties of high-defect phases will differ from those of a Fermi liquid.

One further possible intermediate (microemulsion) phase is proposed in Ref. [79]. Numerous intermediate phases predicted in Ref. [79] can be realized under special conditions, namely, in the presence of a metal electrode (gate) located at a considerable distance, $n_s D^2 \gg 1$, from a two-dimensional layer. The characteristic size of the microemulsion phase apparently exceeds D in this case. The above-mentioned electron concentrations typical of Wigner crystallization in the pure limit suggest, together with the characteristic distances to the gate in actually existing structures (100 nm), that standard structures currently under investigation are hardly likely to exhibit this type of intermediate phase.

In one candidate intermediate phase, the many-particle electronic function has the properties of both a crystal and a liquid [80, 81]. For example, the density–density correlation function, which is the joint probability of finding one electron at point r and at the same time finding the second electron at zero, has maxima at the sites of the triangular crystal lattice (as in a crystal) but does not vanish between them, which is reminiscent of a liquid. Such a wave function corresponds to a liquid of quasiparticles whose mass increases with increasing interaction [82, 83]. A Monte Carlo calculation showed that in a system of spin-polarized one-valley carriers this system can be the ground state in the interval $30 < r_s < 80$. The critical concentration that determines the transition boundary between the liquid phase and the hybrid intermediate phase predicted in Ref. [80] can, in principle, be found from the change in Fermi surface symmetry from circular to hexagonal.

12. Conclusion

Despite much work having been done, both theoretical and experimental, the subject of quantum melting can hardly be

considered closed. Outlined below are some of the questions that remain open.

(1) First, there is the question of the solid–liquid phase boundary in the (n_s, B) plane. No conclusive theoretical predictions exist on the behavior of the boundary, even for the case of an ideal Wigner crystal in a perfect electron system that allows for competition between the integer and fractional Hall effects. Which of the following can be expected to occur: boundary oscillations or, as experiments in Ref. [22] suggest, the penetration of fractal quantum liquids into the solid phase region?

There are no theoretical predictions regarding the behavior of the boundary in a real two-dimensional solid phase stimulated by impurities.

It remains unclear why the slope of the boundary in strong magnetic fields is not universal.

A further unknown is the role of polycrystallinity in the solid phase of actual electron systems.

(2) There is no experimental information on crystallization and quantum melting in systems of topical interest (two-layer graphene, strongly spin–orbit coupled two-dimensional systems, and two-layer systems).

(3) There is no definite experimental information on intermediate phases between a classical quantum liquid and a crystal.

Further experimental progress requires far more perfect structures than currently available.

Acknowledgments

The authors would like to thank E V Devyatov, V M Pudalov, A A Shashkin, and A V Chaplik for their critical remarks, useful discussions, and advice. The work was partially supported by RFBR (grants 15-02-03537 and 16-02-00404), RAS and the RF Ministry of Education and Science.

References

1. Wigner E *Phys. Rev.* **46** 1002 (1934)
2. Monarkha Yu P, Sivokon' V E *Low Temp. Phys.* **38** 1067 (2012); *Fiz. Nizk. Temp.* **38** 1355 (2012)
3. Chaplik A V *Sov. Phys. JETP* **35** 395 (1972); *Zh. Eksp. Teor. Fiz.* **62** 746 (1972)
4. Lindemann F A *Phys. Z.* **11** 609 (1910)
5. Landau L D, Lifshitz E M *Statistical Physics* Vol. 1 (Oxford: Pegramon Press, 1980); Translated from Russian: *Statisticheskaya Fizika* 2nd ed. (Moscow: Fizmatgiz, 1964)
6. Sólyom J *EPJ Web of Conf.* **78** 01009 (2014)
7. Kukushkin I V, Timofeev V B *Adv. Phys.* **45** 147 (1996)
8. Jang J et al. *Nature Phys.* **13** 340 (2017); arXiv:1604.06220
9. Fukuyama H *Solid State Commun.* **17** 1323 (1975)
10. Lozovik Yu E, Yudson V I *JETP Lett.* **22** 11 (1975); *Pis'ma Zh. Eksp. Teor. Fiz.* **22** 26 (1975)
11. Bedanov V M, Gadiyak G V, Lozovik Yu E *Sov. Phys. JETP* **61** 967 (1985); *Zh. Eksp. Teor. Fiz.* **88** 1622 (1985)
12. Tanatar B, Ceperley D *Phys. Rev. B* **39** 5005 (1989)
13. Chui S T, Esfarjani K *Europhys. Lett.* **14** 361 (1991)
14. Chui S T, Tanatar B *Phys. Rev. Lett.* **74** 458 (1995)
15. Pudalov V M et al. *Phys. Rev. Lett.* **70** 1866 (1993)
16. Khodel V A, Shaginyan V R *JETP Lett.* **51** 553 (1990); *Pis'ma Zh. Eksp. Teor. Fiz.* **51** 488 (1990)
17. Amusia M Ya et al. *Theory of Heavy-Fermion Compounds*: *Theory of Strongly Correlated Fermi-Systems* (New York: Springer, 2014)
18. Dolgopolov V T *JETP Lett.* **101** 282 (2015); *Pis'ma Zh. Eksp. Teor. Fiz.* **101** 300 (2015)
19. Fleury G, Waintal X *Phys. Rev. B* **81** 165117 (2010)
20. Pudalov V M, Gershenson M, Kojima H, in *Fundamental Problems of Mesoscopic Physics*: *Interactions and Decoherence* (NATO Science Ser. II, Vol. 154, Eds I V Lerner, B L Altshuler, Y Gefen) (NATO Sci. Series) (Dordrecht: Springer Science + Business Media, 2004) p. 309
21. Lam P K, Girvin S M *Phys. Rev. B* **30** 473(R) (1984)
22. Jiang H W et al. *Phys. Rev. B* **44** 8107 (1991)
23. D'Iorio M, Pudalov V M, Semenchinsky S G *Phys. Rev. B* **46** 15992 (1992)
24. Shashkin A A, Kravchenko G V, Dolgopolov V T *JETP Lett.* **58** 220 (1993); *Pis'ma Zh. Eksp. Teor. Fiz.* **58** 215 (1993)
25. D'Iorio M, Pudalov V M, Semenchinsky S G *Phys. Lett. A* **150** 422 (1990)
26. Kukushkin I V, Timofeev V B *Phys. Usp.* **36** 549 (1993); *Usp. Fiz. Nauk* **163** (7) 1 (1993)
27. Ulinich F P, Usov N A *Sov. Phys. JETP* **49** 147 (1979); *Zh. Eksp. Teor. Fiz.* **76** 288 (1979)
28. Yoshioka D *J. Phys. Soc. Jpn.* **53** 3740 (1984)
29. Yoshioka D *J. Phys. Soc. Jpn.* **55** 885 (1986)
30. Platzman P M, in *The Physics of the Two-Dimensional Electron Gas* (Eds T J Devreese, F M Peeters) (NATO ASI Ser., Ser. B, Vol. 157) (New York: Plenum Press, 1987) p. 97
31. Zhu X, Louie S G *Phys. Rev. Lett.* **70** 335 (1993)
32. Qiu R L J et al., arXiv:1509.07463
33. Shashkin A A et al. *Phys. Rev. Lett.* **73** 3141 (1994)
34. Stormer H L, Willett R L *Phys. Rev. Lett.* **62** 972 (1989)
35. Jiang H W et al. *Phys. Rev. Lett.* **65** 633 (1990)
36. Goldman V J et al. *Phys. Rev. Lett.* **65** 2189 (1990)
37. Williams F I B et al. *Phys. Rev. Lett.* **66** 3285 (1991)
38. Li Y P et al. *Phys. Rev. Lett.* **67** 1630 (1991)
39. Jiang H W et al. *Phys. Rev. B* **44** 8107 (1991)
40. Khrapai V S et al. *Phys. Rev. Lett.* **100** 196805 (2008)
41. Kravchenko S V et al. *Phys. Rev. Lett.* **75** 910 (1995)
42. Pudalov V M, D'lorio M, Campbell J W *JETP Lett.* **57** 608 (1993); *Pis'ma Zh. Eksp. Teor. Fiz.* **57** 592 (1993)
43. Pudalov V M, in *Physics of the Electron Solid* (Conf. Proc. and Lecture Notes in Applied Physics, Vol. 1, Ed. S T Chui) (Cambridge, MA: International Press, 1994)
44. Holmes S N et al. *J. Phys. Condens. Matter* **20** 472207 (2008)
45. Kononov A et al. *Phys. Rev. B* **86** 125304 (2012)
46. Dahal H P et al. *Phys. Rev. B* **74** 233405 (2006)
47. Dolgopolov V T *Phys. Usp.* **57** 105 (2014); *Usp. Fiz. Nauk* **184** 113 (2014)
48. Zhang C-H, Joglekar Y N *Phys. Rev. B* **75** 245414 (2007)
49. Zhang C-H, Joglekar Y N *Phys. Rev. B* **77** 205426 (2008)
50. Côté R, Jobidon J-F, Fertig H A *Phys. Rev. B* **78** 085309 (2008)
51. Dahal H P et al., arXiv:0706.1689
52. Silvestrov P G, Recher R *Phys. Rev. B* **95** 075438 (2017); arXiv:1602.02777
53. Silvestrov P G, Entin-Wohlman O *Phys. Rev. B* **89** 155103 (2014)
54. Berg E, Rudner M S, Kivelson S A *Phys. Rev. B* **85** 035116 (2012)
55. Falko V I *Phys. Rev. B* **49** 7774 (1994)
56. Esfarjani K, Kawazoe Y *J. Phys. Condens. Matter* **7** 7217 (1995)
57. Goldoni G, Peeters F M *Phys. Rev. B* **53** 4591 (1996)
58. Schweigert I V, Schweigert V A, Peeters F M *Phys. Rev. Lett.* **82** 5293 (1999)
59. Weis J-J, Levesque D, Jorge S *Phys. Rev. B* **63** 045308 (2001)
60. Messina R, Löwen H *Phys. Rev. Lett.* **91** 146101 (2003)
61. Oguz E C, Messina R, Lowen H *Europhys. Lett.* **86** 28002 (2009)
62. Lobaskin V, Netz R R *Europhys. Lett.* **77** 38003 (2007)
63. Šamaj L, Trizac E *Phys. Rev. B* **85** 205131 (2012)
64. Schweigert I V, Schweigert V A, Peeters F M *Phys. Rev. B* **60** 14665 (1999)
65. Narasimhan S, Ho T-L *Phys. Rev. B* **52** 12291 (1995)
66. Andrei E Y et al. *Phys. Rev. Lett.* **60** 2765 (1988)
67. Stormer H L, Willett R L *Phys. Rev. Lett.* **68** 2104 (1992)
68. Shashkin A A, Dolgopolov V T, Kravchenko G V *Phys. Rev. B* **49** 14486 (1994)

69. Buhmann H et al. *Phys. Rev. Lett.* **65** 1056 (1990)
70. Li C-C et al. *Phys. Rev. B* **61** 10905 (2000)
71. Ye P D et al. *Phys. Rev. Lett.* **89** 176802 (2002)
72. Chen Y P et al. *Phys. Rev. Lett.* **93** 206805 (2004)
73. Wang Z et al. *Phys. Rev. Lett.* **99** 136804 (2007)
74. Doveston J B et al. *Physica E* **12** 296 (2002)
75. Wang Z et al. *Phys. Rev. B* **85** 195408 (2012); arXiv:1101.2436
76. Drichko I L et al. *Solid State Commun.* **213–214** 46 (2015)
77. Andreev A F, Lifshitz I M *Sov. Phys. JETP* **29** 1107 (1969); *Zh. Eksp. Teor. Fiz.* **56** 2057 (1969)
78. Halperin B I, Nelson D R *Phys. Rev. Lett.* **41** 121 (1978)
79. Spivak B, Kivelson S A *Phys. Rev. B* **70** 155114 (2004)
80. Falakshahi H, Waintal X *Phys. Rev. Lett.* **94** 046801 (2005)
81. Waintal X *Phys. Rev. B* **73** 075417 (2006)
82. Dolgopolov V T *JETP Lett.* **76** 377 (2002); *Pis'ma Zh. Eksp. Teor. Fiz.* **76** 437 (2002)
83. Dolgopolov V T, Shashkin A A *JETP Lett.* **95** 570 (2012); *Pis'ma Zh. Eksp. Teor. Fiz.* **95** 648 (2012)